Design of Extended Weil Code Families via Goldbach-Based Prime Concatenation for LEO-PNT Systems

Jae Duk Yoo , Seungsoo Yoo , Ju-Hyun Maeng , Gyu-In Jee , Sun Yong Kim *

Posted Date: 25 March 2026

doi: 10.20944/preprints202603.1919.v1

Keywords: LEO-based navigation system; PN code; goldbach conjecture; weil family

 doi:10.20944/preprints202603.1919.v1

Article

Design of Extended Weil Code Families via Goldbach-Based Prime Concatenation for LEO-PNT Systems

Jae Duk Yoo [1], Seungsoo Yoo [2], Ju-Hyun Maeng [3], Gyu-In Jee [2] and Sun Yong Kim [2,*]

[1] Department of Electrical, Information and Communication Engineering, Konkuk University, Seoul 05029, Republic of Korea
[2] Department of Electrical and Electronics Engineering, Konkuk University, Seoul 05029, Republic of Korea
[3] Korea Aerospace Research Institute, Daejeon 34133, Republic of Korea
* Correspondence: kimsy@konkuk.ac.kr

Abstract

The Low Earth Orbit (LEO)-based Positioning, Navigation, and Timing (PNT) System has been proposed as an attractive global navigation system because of its strong transmission power and convergence of Precise Point Positioning (PPP). However, constructing a PN family satisfies the constellation size of the LEO-PNT System while maintaining a correlation performance is a major challenge. In this paper, we propose the extended Weil family, constructed by concatenating two Weil sequences based on the Goldbach conjecture. Among 157 prime pairs capable of generating balanced 10,230-chip codes, the prime pair ($p = 10091, q = 139$) yields the largest number of candidate codes satisfying the auto-correlation function (ACF) threshold of BeiDou Navigation Satellite System (BDS) B1 Civil (B1C) family. Using this pair, the total of 254 codes satisfy the BDS B1C correlation thresholds, approximately twice the size of the B1C family. We conducted additional experiments with relaxed cross-correlation function (CCF) thresholds to achieve the target family size of 588, providing two codes for each of the 294 satellites. As a result, a total of 608 codes satisfy the ACF threshold of the BDS B1C family and the CCF threshold of the Global Positioning System (GPS) L1 Civil (L1C) Family, which is sufficient to support the LEO-PNT System.

Keywords: LEO-based navigation system; PN code; goldbach conjecture; weil family

1. Introduction

The Radio Navigation Satellite System (RNSS), which includes global coverage system such as Global Positioning System (GPS), BeiDou Navigation Satellite System (BDS) and regional coverage system such as Navigation with Indian Constellation (NavIC), have served as the cornerstones of positioning, navigation, and timing (PNT) for decades [1]. Despite their performance, the emergence of next-generation technologies demands PNT capabilities that overcome the performance limits of conventional RNSS [2]. For instance, the approximately 10 m positional accuracy of standalone RNSS without augmentation is insufficient for the sub-meter precision required by autonomous vehicles. In addition, the vulnerability of RNSS signals, characterized by low power and susceptibility to signal blockage in urban canyons or intentional interference such as jamming and spoofing, poses challenges for mission-critical applications.

To address these limitations, Low Earth Orbit (LEO)-based PNT systems have been proposed as robust augmentation solutions [3–9]. Unlike Medium Earth Orbit (MEO), Geosynchronous Earth Orbit (GEO) and Inclined Geosynchronous Earth Orbit (IGSO) satellites in RNSS, which operate at altitudes of approximately 20,000 km (MEO) or higher (GEO, IGSO), LEO satellites orbit at significantly lower altitudes, typically between 300 km and 1,200 km. This proximity results in a substantial increase in the minimum received signal power and faster geometric changes compared to those of RNSS. As a representative example, the Pulsar LEO constellation developed by Xona Space Systems provides a minimum signal power of -144.9 dBW for its Pulsar X5 signal, which is 9.1 dB higher than that

 doi:10.20944/preprints202603.1919.v1

of the GPS L5 signal (−154.0 dBW). The maximum relative speed of a Pulsar satellite is 6,327 m/s, which is approximately 8.3 times higher than that of a GPS satellite (765 m/s). These characteristics offer distinct advantages for navigation. First, rapid geometric changes of LEO satellites improve geometric diversity and accelerate convergence of Precise Point Positioning (PPP) [10–12]. Second, the higher received signal power can support positioning in harsh environments, including intentional interference conditions. In several live-sky jamming events, the Pulsar X5 signal demonstrated the ability to reduce the effective radius of a jammer by a factor of 6.3 compared to GPS L5 [13].

Driven by these advantages, numerous organizations are actively developing dedicated LEO-PNT constellations (Table 1). These systems generally fall into two categories: stand-alone PNT systems and information augmentation systems. While a stand-alone PNT system aims to serve navigation services independently of RNSS, an information augmentation system focuses on providing messages to augment the performance of RNSS PNT service. Despite their distinct operational objectives, both types of modern LEO-PNT systems, such as Pulsar, TrustPoint, CentiSpace, and European Space Agency (ESA) LEO-PNT, employ Code Division Multiple Access (CDMA) Direct Sequence Spread Spectrum (DSSS) to ensure interoperability with legacy RNSS. This represents a difference from early LEO-based positioning services, such as the Iridium Satellite, Time, and Location (STL), which utilized independent signal structures. This CDMA-based approach implies that each LEO satellite must be assigned at least one unique Pseudo-Noise (PN) code [14].

Table 1. Overview and comparison of modern dedicated LEO-PNT constellations and their architectures.

Constellation	Country	Status	System Type	Full Operational Capability	Ref.
Iridium STL	USA	Active	Stand-Alone	66	[3,4]
Pulsar	USA	Deploying	Stand-Alone	258	[5,6]
TrustPoint	USA	Demo/Planned	Stand-Alone	384	[7]
CentiSpace	China	Deploying	Augmentation	190	[3,8]
GeeSpace	China	Deploying	Augmentation	240	[3]
ESA LEO-PNT	Europe	In-Orbit Demonstration	Augmentation	11 (IOD)	[3,9]
ArkEdge	Japan	Feasibility	Augmentation	480	[3]

* The constellation size corresponds to the full operational capability.

Historically, a variety of PN sequences have been proposed to meet these multiple-access requirements. The Gold, Kasami, Bent and No sequences all have a period of $2^n - 1$ for some integer n [15–18]. The Z_4-linear sequences have twice the previous ones, such as $2(2^n + 1)$ [19]. The Weil sequence has an odd prime period p [20]. Among these, the GPS L1 Coarse/Acquisition (C/A) signal, one of the first-generation GPS signals, adopted the Gold sequence with a period of $2^{10} - 1$ (1,023 chips) [21].

Recent modernized signals, such as GPS L1 Civil (L1C), GPS L2 Civil (L2C) Civil Moderate (CM) / Civil Long, GPS L5, BDS B1 In-phase (B1I), BDS B1 Civil (B1C), BDS B2a, BDS Precise Point Positioning (PPP)-B2b, BDS B3 In-phase (B3I), NavIC L1 Standard Positioning Service (SPS) and Pulsar X5, employ longer sequence periods. Although each of these signals has its own Interface Control Document (ICD), this paper selectively cites five specific ICDs [21–25], as they are individually selected to represent each of the distinct generation architectures discussed. To ensure backward compatibility with this foundational GPS L1 C/A signal, modern navigation signals from GNSS and LEO-PNT systems are intentionally designed with sequence periods that are integer multiples of 1,023 chips. With a code length of 10,230 chips, these signals offer an additional 10 dB of processing gain compared to the legacy GPS L1 C/A signal. However, constructing a 10,230-chip sequence presents a challenge, as it differs from the natural period of sequences. Therefore, these PN families are constructed using modification

 doi:10.20944/preprints202603.1919.v1

techniques, such as a truncated maximal-length sequence (m-sequence), extended Gold sequence, padded Weil sequence, truncated Weil sequence, and interleaved Z_4 (IZ4) sequence, to satisfy their design criteria [26–30] (Table 2).

Table 2. Summary of sequence generation architectures employed in the PN families of modern navigation signals.

Signal Type	Code Type	Frequency Band (MHz)	Period N	# of 1,023
GPS L1 C/A	Gold	1575.42 (L1)	1,023	1
NavIC S SPS	Gold	2492.03 (S)	1,023	1
NavIC L5 SPS	Gold	1176.45 (L5)	1,023	1
Pulsar X1 Primary Code	Kasami / Gold	1593.32 (L1)	1,023	1
BDS B1I	Truncated Gold	1561.10 (L1, B1)	2,046	1
GPS L2C CM	Truncated m-sequence	1227.60 (L2)	10,230	10
GPS L5	Extended Gold	1176.45 (L5)	10,230	10
BDS B2a	Extended Gold	1176.45 (L5, B2)	10,230	10
BDS PPP-B2b	Extended Gold	1176.45 (L5, B2)	10,230	10
BDS B3I	Extended Gold	1268.52 (L2, B3)	10,230	10
Pulsar X5 Primary Code	Extended Gold	1190.52 (L5)	10,230	10
GPS L1C	7-chip Padded Weil	1575.42 (L1)	10,230	10
BDS B1C	13-chip Truncated Weil	1575.42 (L1, B1)	10,230	10
NavIC L1 SPS	Interleaved Z_4 Linear (IZ4)	1575.42 (L1)	10,230	10
GPS L2C CL	Truncated m-sequence	1227.60 (L2)	767,250	750

Such structural modifications lead to non-ideal correlation properties compared to naturally periodic sequences. As a result, only a subset of codes with acceptable correlation performance can be selected from the entire family, inherently reducing the effective family size. A detailed analysis of the correlation degradation introduced by these structural modifications is provided in Section 2.2 and Section 3.2. This reduction poses a significant challenge for LEO-PNT systems. Since LEO constellations operate at low altitudes and require hundreds of satellites for continuous coverage, the remaining subset of codes is often insufficient to support such large-scale constellations. To address this, Wang et al. [31] proposed an assignment method in which several satellites share the same PN code based on their geographical isolation and demonstrated the feasibility of this approach. In addition, the Pulsar identifies individual satellites using a hierarchical structure of 18 primary codes and 16 overlay codes [6]. The detailed PN code assignment method and signal structure of the Pulsar are discussed in Section 2.3. Although these PN code assignment methods offer advantages, such as reducing the receiver's computational buffer and enabling efficient code assignment for large-scale constellations, these methods depend on sufficient geographical and Doppler isolation between satellites sharing the same code. This prerequisite makes them vulnerable to interference in dense environments, thereby severely limiting their scalability for future massive LEO constellations.

To address these requirements, we propose an extended Weil family constructed via prime concatenation, targeting a family size of 588 codes, corresponding to two unique codes per satellite for a LEO constellation with 294 satellites. Our design criteria are established based on the Xona Pulsar X5 signal to ensure practical applicability, the details of which are discussed in Section 3.1. This proposed extended Weil family, termed the Concatenated Weil (C.W.) family, is motivated by the Goldbach conjecture, which states that every even integer greater than 2 can be expressed as the sum of two primes [32]. Using this property, we construct C.W. codes for period N (e.g. 10,230) by concatenating two Weil codes generated from prime periods p and q such that $N = p + q$. When both p and q satisfy

 doi:10.20944/preprints202603.1919.v1

$p \equiv 3 \pmod 4$ and $q \equiv 3 \pmod 4$, both Weil sequences exhibit a fixed imbalance of -1 [33]. As a result, a global phase inversion of one segment restores the exact balance of 0. From the 157 prime pairs capable of generating balanced codes, we select the optimal prime pair based on the number of candidate codes. Finally, we evaluated the proposed C.W. codes generated under two different thresholds, benchmarking their performance against modern PN families, specifically that of the GPS L1C, BDS B1C, and NavIC L1 SPS.

This paper is organized as follows: Section 2 introduces the performance metrics for PN families and provides an overview of existing 10,230-chip PN families used in GPS, BDS and NavIC civil signals. Furthermore, it details the signal structure and hierarchical code assignment of the Pulsar, a representative LEO-PNT constellation. Section 3 establishes the design criteria based on the Pulsar X5 signal specifications and presents the proposed C.W. family, covering the construction method, the criteria for selecting the optimal prime number pair, and the procedure for searching for good codes. Section 4 presents a comparative performance analysis of the proposed C.W. family versus the modern PN families. Finally, Section 5 discusses the limitation of the study and Section 6 concludes the paper.

2. Background

2.1. Performance Measurement

Most satellite navigation systems, including GPS, BDS, NavIC, Pulsar, TrustPoint, CentiSpace, and ESA LEO-PNT, broadcast signals modulated by message bits and spread by PN codes in the time domain [1,14]. Therefore, a PN family must be optimized for both even correlation, which occurs in the absence of message bit transitions within an integration interval, and odd correlation, which occurs in the presence of transitions within an integration interval. The even correlation function R and the odd correlation function $\hat{R}$ for the two bipolar sequences (± 1-valued) $\boldsymbol{a}$ and $\boldsymbol{b}$ of period N are defined as follows:

$$R(\boldsymbol{a},\boldsymbol{b},\tau) = \sum_{i=0}^{N-1} a_i b_{i+\tau}, \qquad \hat{R}(\boldsymbol{a},\boldsymbol{b},\tau) = \sum_{i=0}^{N-\tau-1} a_i b_{i+\tau} - \sum_{i=N-\tau}^{N-1} a_i b_{i+\tau}, \tag{1}$$

where a_i and b_i denote the elements of $\boldsymbol{a}$ and $\boldsymbol{b}$ with indices computed modulo the period N, and τ is the integer code shift in the range $0 \le \tau < N$. The correlation function of a code with itself is referred to as the auto-correlation function (ACF), whereas the correlation function between two distinct codes is referred to as the cross-correlation function (CCF). The sidelobes correspond to the correlation values obtained when the codes are not perfectly synchronized. For the ACF, all values at non-zero shifts ($\tau \neq 0$) constitute the sidelobes, while for the CCF, every correlation value is considered a sidelobe. The maximum magnitude of these sidelobes serves as a performance metric to evaluate the PN family. Consequently, the normalized maximum sidelobe power, denoted as $P_{\mathrm{ACF_E}}$ (Even ACF), $P_{\mathrm{ACF_O}}$ (Odd ACF), $P_{\mathrm{CCF_E}}$ (Even CCF) and $P_{\mathrm{CCF_O}}$ (Odd CCF), are defined as follows:

$$P^{(i)}_{\mathrm{ACF_E}} = \frac{\max\limits_{0<\tau<N} \left\{ |R(\boldsymbol{s}^{(i)},\boldsymbol{s}^{(i)},\tau)|^2 \right\}}{N^2}, \qquad P^{(i,j)}_{\mathrm{CCF_E}} = \frac{\max\limits_{0\le\tau<N} \left\{ |R(\boldsymbol{s}^{(i)},\boldsymbol{s}^{(j)},\tau)|^2 \right\}}{N^2}, \tag{2}$$

$$P^{(i)}_{\mathrm{ACF_O}} = \frac{\max\limits_{0<\tau<N} \left\{ |\hat{R}(\boldsymbol{s}^{(i)},\boldsymbol{s}^{(i)},\tau)|^2 \right\}}{N^2}, \qquad P^{(i,j)}_{\mathrm{CCF_O}} = \frac{\max\limits_{0\le\tau<N} \left\{ |\hat{R}(\boldsymbol{s}^{(i)},\boldsymbol{s}^{(j)},\tau)|^2 \right\}}{N^2}, \tag{3}$$

where $\boldsymbol{s}^{(i)}$ and $\boldsymbol{s}^{(j)}$ denote the two distinct codes in the PN family S, where $i \neq j$. Assuming independent navigation data bits, the even and odd correlation scenarios are equally likely to occur. Therefore, we evaluated the PN family using the combined metrics $P_{\mathrm{ACF_M}}$ and $P_{\mathrm{CCF_M}}$, which approximate the expected sidelobe power under random data transitions by averaging the two cases equally. This is calculated as the arithmetic mean of the even and odd correlation powers, defined as follows:

$$P^{(i)}_{\mathrm{ACF_M}} = \frac{P^{(i)}_{\mathrm{ACF_E}} + P^{(i)}_{\mathrm{ACF_O}}}{2}, \qquad P^{(i,j)}_{\mathrm{CCF_M}} = \frac{P^{(i,j)}_{\mathrm{CCF_E}} + P^{(i,j)}_{\mathrm{CCF_O}}}{2}, \tag{4}$$

 doi:10.20944/preprints202603.1919.v1

While the maximum sidelobes of the PN family show the theoretical worst-case interference, such an event requires a specific combination of relative code phase, data bit transitions, and visible satellites. In an operational environment, these worst-case conditions are unlikely to occur simultaneously. Therefore, we analyze the statistical distribution of $P_{\mathrm{ACF_M}}$ and $P_{\mathrm{CCF_M}}$ to evaluate the performance of the PN family S. Leaving K denote the total number of sequences in S, the means (μ) of these metrics across the entire family are defined as follows:

$$P_{\mu_{\mathrm{ACF}}} = \frac{1}{K}\sum_{i=1}^{K} P^{(i)}_{\mathrm{ACF_M}}, \qquad P_{\mu_{\mathrm{CCF}}} = \frac{1}{K(K-1)}\sum_{i=1}^{K}\sum_{\substack{j=1 \\ i\neq j}}^{K} P^{(i,j)}_{\mathrm{CCF_M}} \tag{5}$$

For practical analysis and visualization, all the aforementioned metrics calculated in the linear power scale are subsequently converted to the decibel (dB) scale. Throughout the remainder of this paper, the prefix P is omitted, and the same symbol without P denotes the metric expressed in dB. Let P_X represent any of the defined linear power metrics (e.g. $P_{\mathrm{ACF_E}}$, $P_{\mathrm{CCF_M}}$ or $P_{\mu_{\mathrm{ACF}}}$); its equivalent representation in the dB scale, simply denoted as X (e.g. $\mathrm{ACF_E}$, $\mathrm{CCF_M}$, or μ_{ACF}), is expressed as follows:

$$X = 10\log_{10}(P_X). \tag{6}$$

The balance property (B) of a bipolar sequence $\boldsymbol{s}$ is the difference between the number of $+1$'s and the number of -1's within a period. Minimizing the absolute value of B is desirable for suppressing the direct current (DC) component in the signal's power spectral density. Consequently, achieving $\mathrm{B} \approx 0$ is a fundamental criterion for evaluating the efficiency and robustness of the PN family in RNSS communication environments. It is defined as the sum of the elements:

$$\mathrm{B} = \sum_{i=0}^{N-1} s_i \tag{7}$$

2.2. Conventional Sequences

As previously discussed, the truncated m-sequences, extended Gold sequences, padded Weil sequences, truncated Weil sequences and IZ4 sequences are typically employed to construct a PN family with a length of 10,230 chips [26–30]. In this section, we summarize the detailed construction of each family. Although the primary code of the Pulsar X5 signal, the reference signal for our criteria, is known to utilize extended Gold sequences, the exact generation polynomials have not been publicly disclosed [5,6]. Therefore, this section focuses on the standard codes adopted in RNSS civil signals (Table 3).

The GPS L2C signal utilizes a truncated m-sequence generated by a 27-bit Linear Feedback Shift Register (LFSR) for its PN family [21,26]. The family is formed by truncating the $2^{27}-1$ period of the m-sequence to a fixed length using a periodic reset. Each k-th sequence is distinguished by a delay $\tau^{(k)}$, determined by the initial state of the LFSR.

The extended Gold sequence serves as the PN sequence for various RNSS signals, such as the GPS L5, BDS B2a, BDS PPP-B2b, and BDS B3I signals [22,27]. These codes are generated using a preferred pair of 13-bit m-sequences, denoted G_1 and G_2. A distinct feature of this family is the short-cycle technique applied to the G_1 register. While the G_2 register follows its natural period of 8,191 chips, the G_1 register is reset to its initial state after 8,190 chips. At the end of the 10,230-chip period, the PN generator resets the entire register. The specific k-th code is determined by the initial phase $\tau^{(k)}$ of the G_2 register.

A Weil sequence is generated based on Legendre sequences, denoted L_p, which have an odd prime length p [20]. The definitions of Legendre sequences are based on the concept of the modulo quadratic residue p [34]. If any integer x exists such that the congruence $x^2 \equiv t \pmod{p}$ for t, a t is

 doi:10.20944/preprints202603.1919.v1

defined as the quadratic residue modulo p. Based on this, the elements of the Legendre sequence are determined as follows:

$$L_p(t) = \begin{cases} 0 & \text{if } t \equiv 0 \pmod{p} \\ +1 & \text{if } t \text{ is a quadratic residue modulo } p \\ -1 & \text{if } t \text{ is a non-quadratic residue modulo } p \end{cases}, \tag{8}$$

Table 3. Detailed construction parameters of the 10,230-chip PN families.

Signal		Polynomial	PN Generation	Parameter of Code Index k
GPS L2C CM	c	$x^{27}+x^{24}+x^{21}+x^{19}+x^{16}+x^{13}+x^{11}+x^9+x^6+x^5+x^4+x^3+1$	$c(t+\tau^{(k)})$	$\tau^{(k)}$
GPS L5	G_1	$x^{13}+x^{12}+x^{10}+x^9+1$	$G_1(t)\oplus G_2(t+\tau^{(k)})$	$\tau^{(k)}$
	G_2	$x^{13}+x^{12}+x^8+x^7+x^6+x^4+x^3+x+1$		
BDS B2a$_d$	G_1	$x^{13}+x^{11}+x^5+1$	$G_1(t)\oplus G_2(t+\tau^{(k)})$	$\tau^{(k)}$
	G_2	$x^{13}+x^{12}+x^{11}+x^9+x^5+x^3+1$		
BDS B2a$_p$	G_1	$x^{13}+x^7+x^6+x^3+1$	$G_1(t)\oplus G_2(t+\tau^{(k)})$	$\tau^{(k)}$
	G_2	$x^{13}+x^{12}+x^8+x^7+x^5+x+1$		
BDS PPP-B2b	G_1	$x^{13}+x^{10}+x^9+1$	$G_1(t)\oplus G_2(t+\tau^{(k)})$	$\tau^{(k)}$
	G_2	$x^{13}+x^{12}+x^9+x^6+x^4+x^3+1$		
BDS B3I	G_1	$x^{13}+x^4+x^3+x+1$	$G_1(t)\oplus G_2(t+\tau^{(k)})$	$\tau^{(k)}$
	G_2	$x^{13}+x^{12}+x^{10}+x^9+x^7+x^6+x^5+x+1$		
GPS L1C	Weil	$W_p = L_p(t)L_p(t+t_w^{(k)}),\quad (p=10223)$	Insert fixed code at $i_p^{(k)}-1$ chip of W_p	$t_w^{(k)}, i_p^{(k)}$
	Fixed	7-chip length fixed sequence (0110100)		
BDS B1C	Weil	$W_p = L_p(t+i_t^{(k)}-1)L_p(t+i_t^{(k)}+t_w^{(k)}-1),\ (p=10243)$	13-chip truncation with W_p	$t_w^{(k)}, i_t^{(k)}$
NavIC L1 SPS	IZ4	Coupled shift registers based on tri-register (55-bit R0, 55-bit R1, 5-bit C)	Interleaved $Z_4 \to$ binary (non-linear mapping)	$IS_{R0}^{(k)}, IS_{R1}^{(k)}, IS_C^{(k)}$
[P] C.W.	Weil	$W_p = L_p(t)L_p(t+t_{w1}^{(k)}),\quad (p=10091)$	Insert q-chip W_q at $i_p^{(k)}-1$ chip of W_p	$t_{w1}^{(k)}, t_{w2}^{(k)}, i_p^{(k)}$
	Weil	$W_q = L_q(t)L_q(t+t_{w2}^{(k)}),\quad (q=139)$		

* Note 1: [P] denotes the proposed method in this work. * Note 2: The detailed construction of the proposed C.W. families are presented in Section 3.

A Weil sequence is constructed by combining the t-th element and the $(t+t_w)$-th element of a Legendre sequence via multiplication (modulo-2 addition for unipolar sequence) [20]. The phase difference between the two elements, t_w, is defined as the Weil index. Each code within a Weil family of length p, denoted as W_p, is distinguished by its specific Weil index t_w. Note that if the prime p satisfies condition $p \equiv 3 (\text{mod } 4)$, the balance property of each code in the family W_p is equal to $L_p(0)$ [33]. The Weil sequence can be summarized as follows:

$$W_p(t) = L_p(t)L_p(t+t_w), \left(1 \le t_w \le \frac{p-1}{2}\right), \tag{9}$$

Unlike the Gold sequence defined by a period 2^n-1 where n denotes the order of the LFSR register, the Weil sequence is based on the prime period, allowing for more flexible sequence construction. The GPS L1C signal adopts a padded Weil family, formed by inserting the fixed unipolar code '0110100' into a 10,223-chip Weil sequence at a predefined insertion index [23,28]. In comparison, the BDS B1C signal employs a truncated Weil family, achieved by removing 13 chips from a 10,243-chip Weil sequence with a truncation index [24,29] (Figure 1). Therefore, both the GPS L1C and BDS B1C families

 doi:10.20944/preprints202603.1919.v1

require two parameters to generate the k-th code: Weil index $t_{\mathrm{w}}^{(k)}$ and insertion index $i_{\mathrm{p}}^{(k)}$ for GPS L1C family, Weil index $t_{\mathrm{w}}^{(k)}$ and truncation index $i_{\mathrm{t}}^{(k)}$ for BDS B1C family.

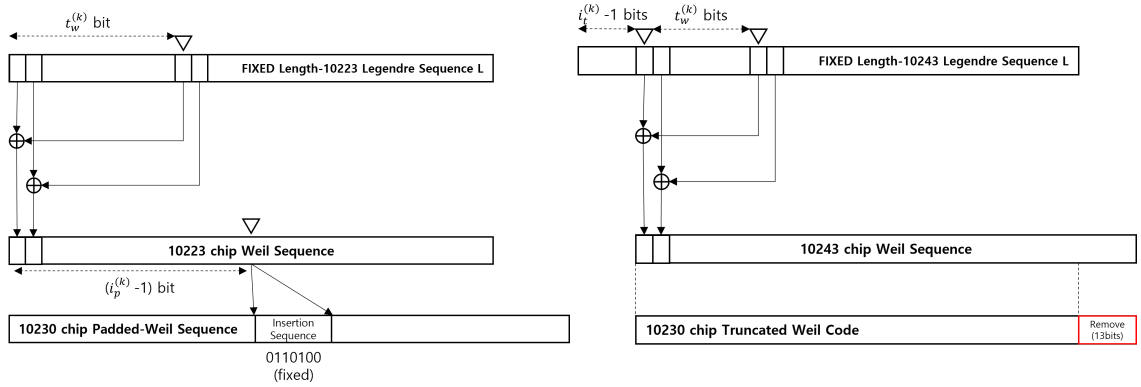

(**a**) (**b**)

Figure 1. Structural comparison of legacy Weil-based PN families illustrating different length-adjustment strategies: (**a**) Padded Weil family of GPS L1C using fixed-code insertion; (**b**) Truncated Weil family of BDS B1C using chip removal.

The NavIC L1 SPS signal employs an IZ4 sequence [25,30]. The IZ4 code is constructed by interleaving five distinct Z_4-linear sequences, where the sequence sets are algebraically determined over Galois rings [19]. The interleaving process itself is orchestrated using the Chinese Remainder Theorem (CRT), seamlessly combining the five sequences, each with a natural period of 2,046 chips, into a unified structure [35]. This architecture exactly achieves the 10,230-chip period without any truncation or padding, thereby preventing the degradation of even correlation performance. The IZ4 sequence family is generated using a coupled shift-register hardware architecture consisting of 55-bit registers R0, R1 and 5-bit register C. The specific k-th code within the family is completely determined by the initial states assigned to these registers, denoted $IS_{\mathrm{R0}}^{(k)}$, $IS_{\mathrm{R1}}^{(k)}$, and $IS_{\mathrm{C}}^{(k)}$.

The method of generating a family of PN significantly influences its correlation properties (Table 4). The truncated m-sequence used in the GPS L2C CM signal exhibits the most degraded mean correlations. In contrast, the extended Gold sequences demonstrate moderate improvements. The most notable contrast lies between the truncated Weil sequence (BDS B1C) and the IZ4 sequence (NavIC L1 SPS). The BDS B1C family achieves the best overall mean ACF (μ_{ACF}) of -31.48 dB. Interestingly, while the IZ4 sequence achieves the lowest even correlation performance ($\mathrm{ACF_E}$ and $\mathrm{CCF_E}$), its overall μ_{ACF} and μ_{CCF} decreased to -30.79 dB and -29.70 dB due to poor odd correlation properties. This specific discrepancy highlights the inherent trade-off of the IZ4 generation method, which interleaves five codes without truncation or padding.

Table 4. Comparison of correlation properties for 10,230-chip PN families from BDS, GPS, and NavIC civil signals, and the proposed C.W. families.

Signal Type	Family Size	Normalized ACF (dB)			Normalized CCF (dB)		
		μ_{ACF}	**Max** $\mathrm{ACF_E}$	**Max** $\mathrm{ACF_O}$	μ_{CCF}	**Max** $\mathrm{CCF_E}$	**Max** $\mathrm{CCF_O}$
GPS L2C CM	63	-28.57	-26.90	-27.21	-28.18	-25.39	-26.08
GPS L5	420	-29.06	-28.56	-26.22	-28.55	-26.36	-25.20
BDS $\mathrm{B2a_d}$	63	-29.32	-29.02	-28.51	-28.54	-25.91	-26.39
BDS $\mathrm{B2a_p}$	63	-29.35	-29.02	-28.51	-28.54	-25.84	-26.22
BDS PPP-B2b	63	-29.29	-28.93	-28.51	-28.54	-25.20	-25.91
BDS B3I	63	-29.08	-28.03	-27.21	-28.60	-25.84	-25.76
GPS L1C	420	-30.38	-31.17	-28.03	-28.57	-27.21	-26.22

 doi:10.20944/preprints202603.1919.v1

Table 4. *Cont.*

Signal Type	Family Size	Normalized ACF (dB)			Normalized CCF (dB)		
		μ_{ACF}	Max ACF_E	Max ACF_O	μ_{CCF}	Max CCF_E	Max CCF_O
BDS B1C	126	−31.48	−31.19	−31.19	−28.86	−27.29	−27.29
NavIC L1 SPS	128	−30.79	−31.70	−29.83	−29.70	−31.70	−26.50
[P] C.W. Thr.A	254	−31.46	−31.19	−31.19	−28.76	−27.29	−27.29
[P] C.W. Thr.B	608	−31.47	−31.19	−31.19	−28.72	−27.21	−26.22

* Note 1: [P] denotes the proposed method in this work. * Note 2: Thr.A and Thr.B denote the threshold criteria defined in Section 3.

2.3. The Pulsar Specification

The Pulsar is a LEO-PNT system designed for standalone PNT services, consisting of approximately 258 satellites deployed at an altitude of 1080 km [5,6]. To ensure seamless global coverage, the constellation is organized into a total of 18 orbital planes: 12 inclined planes (53° inclination, 192 satellites) and 6 polar planes (97° inclination, 66 satellites). This constellation guarantees continuous global coverage with at least three visible satellites assuming a 15° elevation mask, including the polar regions.

The Pulsar signals are designed to be compatible with legacy RNSS receivers by utilizing similar frequency bands and CDMA-DSSS principles. The system broadcasts the X1 signal in the L1 band (1593.3225 MHz) and the X5 signal in the L5 band (1190.51625 MHz). Despite the high transmission power, the center frequencies are slightly offset to prevent interference with existing RNSS systems. Furthermore, an Enhanced Feher's Quadrature Phase Shift Keying (EFQPSK) modulation is adopted for its excellent bandwidth efficiency, thereby minimizing out-of-band spectral emissions [36] (Table 5).

Table 5. Comparison of signal design parameters between GPS and Pulsar in the L1 and L5 bands, adapted from [6].

Parameter		L1 Band		L5 Band	
		Pulsar X1	GPS L1C/A	Pulsar X5	GPS L5
Carrier Frequency		1593.3225 MHz	1575.42 MHz	1190.51625 MHz	1176.45 MHz
Modulation		EFQPSK	BPSK	EFQPSK+CSK[2]	QPSK
Minimum Received Power		−148.2 dBW	−158.5 dBW	−144.9 dBW	−154.0 dBW
Primary Code	**Family**	Kasami and Gold	Gold	Extended Gold	Extended Gold
	Family Size	D:16(K)+2(G)[1] P:16(K)+2(G)	210	D:18 P:18	D:210 P:210
	Chip rate	1.023 Mchip/s	1.023 Mchip/s	10.23 Mchip/s	10.23 Mchip/s
	Code Length	1,023 chip	1,023 chip	10,230 chip	10,230 chip
Overlay Code	**Family**	Memory	-	Memory	Neuman-Hoffman
	Family Size	P:16	-	P:16	-
	Chip rate	1,000 chip/s	-	1,000 chip/s	1,000 chip/s
	Length (pilot)	100 chip	-	100 chip	10 chip
	Length (data)	-	-	-	20 chip
Data	**Symbol Length**	1 ms	20 ms	2 ms	10 ms
	Symbol rate	1,000 symbol/s	50 symbol/s	500 symbol/s	100 symbol/s
	Bit rate	1,000 bit/s	50 bit/s	4,000 bit/s	50 bit/s

* Note 1: (K) label for Kasami sequence and (G) label for Gold sequence. * Note 2: Code Shift Keying (CSK) modulation is employed in Pulsar X5 data channel.

 doi:10.20944/preprints202603.1919.v1

Each signal comprises a data channel and a pilot channel, both of which consist of a carrier, a primary code, and modulating data bits. The data channel is modulated by a navigation message, whereas the pilot channel is modulated by an overlay code. In particular, the data channel of the Pulsar X5 signal uses Code Shift Keying (CSK) modulation [37]. This advanced modulation enables the signal to achieve a high data rate of 500 symbols per second, which corresponds to 4,000 bits per second.

The Pulsar adopts a unique strategy in which all satellites within the same orbital plane share identical primary codes. Specifically, the X1 signal employs the Kasami sequence and Gold sequence as its primary codes, whereas the X5 signal adopts the extended Gold sequence. Since there are 18 orbital planes in the constellation, 18 different pairs of data and pilot primary codes are utilized. Furthermore, each satellite within an orbital plane uses a distinct overlay code, although the same set of overlay codes is reused across different orbital planes. These overlay codes are memory codes, and the same set is used for both X1 and X5 signals. Consequently, the specific combination of a primary code and an overlay code is used to uniquely identify each satellite.

This unique code assignment strategy is feasible because multiple satellites from the same orbital plane are rarely visible to a receiver simultaneously. In fact, simulations based on the Pulsar constellation parameters demonstrate that, given a 15° elevation mask, a maximum of only three satellites from the same orbital plane can be observed at any given time. When these few satellites are concurrently visible, they are spatially distributed far apart along the same orbital track-typically with one ascending, one near the zenith, and one descending. Because of this wide spatial separation, their relative velocity vectors with respect to the receiver are distinctly different, inherently resulting in large Doppler shift differences. This vast separation in the frequency domain effectively prevents cross-correlation interference, even when the same primary code is shared.

3. Methodology

3.1. The PN Family Requirements

The nominal Pulsar architecture mitigates intra-system interference using spatial and Doppler separation [5,6]. However, operational constellations exceed their design size to ensure system redundancy and robust coverage. For example, although the nominal GPS constellation is defined with 24 slots, it currently operates with 31 active satellites [38]. Applying this operational consideration to LEO-PNT systems, a Pulsar constellation designed for 258 satellites will likely require additional satellites beyond its nominal capacity. However, this assignment architecture expands the constellation to force the introduction of entirely new orbital planes rather than utilizing existing ones, resulting in significant deployment overhead and systemic inefficiency.

Therefore, to eradicate the risk of intra-system interference, this study proposes transitioning from a plane-based code assignment to an individualized approach, allocating a unique PN code to every satellite. Although this approach prioritizes the robustness of the system against intra-system interference over minimizing the acquisition complexity at the receiver, the increased computational burden can be mitigated by using external network assistance data, such as aiding acquisition [39]. Operating under this premise, this study expands the target constellation size to 294 satellites, deliberately accommodating two spare satellites within each of the 18 orbital planes. Furthermore, reflecting the signal architecture of the Pulsar, we assume an operational environment where each satellite requires two distinct PN codes: one for the data channel and one for the pilot channel.

We established the PN family design criteria based on the Pulsar architecture and the study by Rushanan [28] on the design of the spreading codes for the GPS L1C signal:

- The PN family is intended to serve as primary codes for the Xona Pulsar X5 signal; therefore, it must maintain compatibility with the 10,230-chip period structure of the baseline X5 signal.
- Taking into account the expanded operational size of the constellation and the signal structure of the Pulsar, a total of 294 pilot and data code pairs are required.
- Given the EFQPSK modulation of the Xona Pulsar, strict synchronized orthogonality (i.e. $\tau = 0$) between the pilot and the data codes within a single satellite is not required.

 doi:10.20944/preprints202603.1919.v1

- The codes must be optimized with both even and odd correlation sidelobes.
- The codes must maintain strict balance (i.e., B $\approx$ 0).
- The PN family must exhibit correlation performance comparable to that of other navigation signals.

3.2. The Concatenated Weil Sequence

This study focuses on the Weil-based approach for two reasons. First, in practical scenarios, a receiver never observes the entire satellite constellation simultaneously [1]. Because only a limited subset of satellites is visible, the operational impact of the maximum CCF sidelobes is inherently mitigated. The probability of encountering sequence pairs with the worst-case correlation is physically restricted, a challenge that can be resolved through sequence assignment techniques, such as the method proposed by Wang et al. [31]. This implies that achieving near-perfect CCF performance, a strength of the IZ4 sequence, is less critical. Second, although the IZ4 sequence exhibits outstanding even correlation metrics, which would be highly advantageous for a CSK modulated data channel, the Pulsar X5 pilot channel does not employ CSK modulation [5,6]. Consequently, both even and odd correlations must be considered equally. When evaluated using μ_{ACF}, the overall performance of the IZ4 sequence is degraded due to its poor odd correlation properties. In contrast, Weil-based sequences demonstrate excellent performance μ_{ACF}. Therefore, the key objective of this research is to maintain the ACF performance inherent to Weil-based sequences while increasing the family size sufficiently to accommodate large-scale LEO-PNT constellations.

A Weil family of prime period p contains $\frac{p-1}{2}$ sequences [20]. However, not all codes satisfy the correlation threshold required for an acceptable code, as defined by the maximum sidelobe after being truncated or padded [23,24,28,29]. Although there are 5,111 distinct Weil codes for period 10,223, only a subset of 480 codes meets the correlation threshold for the GPS L1C signal. From this subset, 420 codes were ultimately selected to construct the final GPS L1C family. In the case of the BDS B1C family, which uses a stricter correlation threshold, only a subset of 126 codes meets the criteria out of a total of 5,121 possibilities. This severe reduction implies that constructing a family of the desired size is difficult to achieve by simply truncating or padding a fixed code. Therefore, we draw inspiration from the concept of the IZ4 sequence, which involves combining two or more distinct codes. The proposed C.W. code is based on two mathematical properties:

1. Based on Goldbach's strong conjecture, every even integer N greater than 2 can be expressed as the sum of two primes, denoted as p and q (i.e., $N = p + q$) [32].
2. Weil sequences exhibit a fixed imbalance of -1 when the period p satisfies $p \equiv 3 \pmod 4$ [33].

Although a formal mathematical proof for Goldbach's strong conjecture remains elusive, it has been empirically verified for all even integers up to $4 \cdot 10^{18}$ by Oliveira e Silva et al. [32]. Because the sequence periods typically required for LEO-PNT and RNSS signals fall well within this verified bound, the conjecture provides a robust and practically guaranteed foundation for our design. Based on this property, for any given even sequence period N, there fundamentally exists a pair of prime numbers p and q satisfying $N = p + q$. This mathematical property guarantees that we can independently construct a family of parents in the p-period Weil family, denoted W_p, and a family of children in the q-period Weil, denoted W_q. The generation expressions for W_p and W_q are defined as follows:

$$W_p(t) = L_p(t)L_p(t + t_{\mathrm{w1}}), \left(1 \le t_{\mathrm{w1}} \le \frac{p-1}{2}\right), \tag{10}$$

$$W_q(t) = L_q(t)L_q(t + t_{\mathrm{w2}}), \left(1 \le t_{\mathrm{w2}} \le \frac{q-1}{2}\right), \tag{11}$$

where L_p and L_q are Legendre sequences of lengths p and q, respectively, and t_{w1} and t_{w2} are the Weil indices of the parent family W_p and the child family W_q. Let $\boldsymbol{w_p} \in W_p$ and $\boldsymbol{w_q} \in W_q$ denote specific codes selected from their respective families. We can construct the C.W. code $\boldsymbol{w}$ with a N-chip period

 doi:10.20944/preprints202603.1919.v1

by inserting $\boldsymbol{w_q}$ into $\boldsymbol{w_p}$. If the periods p and q both satisfy $p \equiv 3 \pmod 4$ and $q \equiv 3 \pmod 4$, the balance properties of the codes in the families W_p and W_q are determined by $L_p(0)$ and $L_q(0)$, which evaluate to -1 in this case [33]. As a result, applying a global phase inversion ϕ (i.e., multiplying by -1 for the bipolar code) to $\boldsymbol{w_q}$ prior to insertion restores the exact balance of 0 for the composite sequence $\boldsymbol{w}$ (Figure 2).

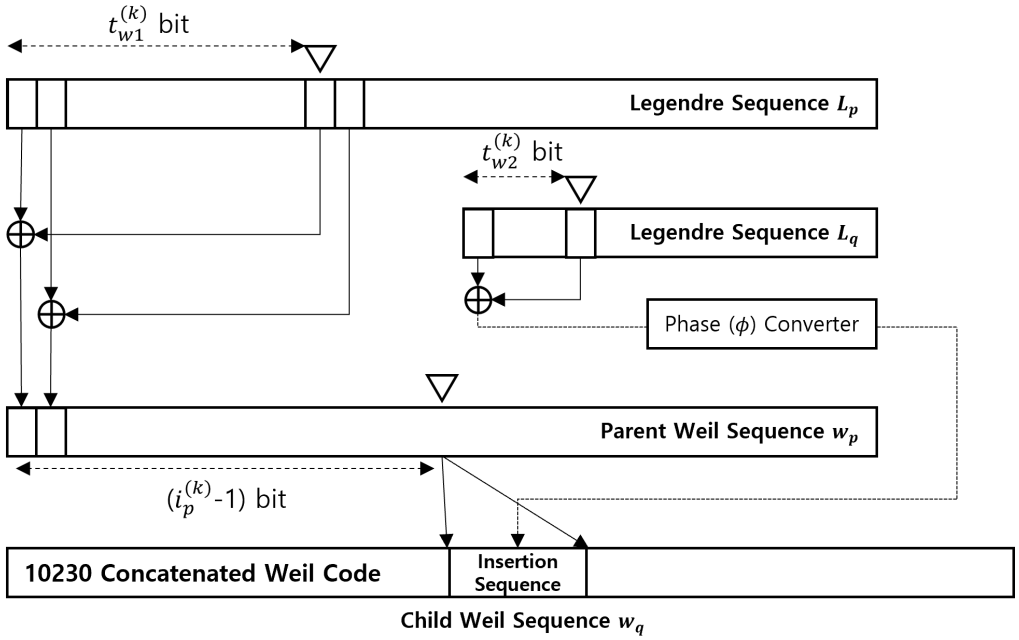

Figure 2. Structural overview of the proposed Concatenated Weil (C.W.) code construction, highlighting the child sequence insertion and the phase inversion mechanism.

The Legendre sequences, L_p and L_q, used to construct the C.W. family, are predetermined sequences shared by all codes within a family. Consequently, a receiver can locally generate the k-th C.W. code using only three parameters: $t_{\mathrm{w1}}^{(k)}$, $t_{\mathrm{w2}}^{(k)}$, and $i_{\mathrm{p}}^{(k)}$. This structural parameterization ensures that the memory complexity required for receiver implementation is equivalent to that of modern state-of-the-art GNSS signals. For context, generating a GPS L1C code requires storing a 10,223-chip Legendre sequence, a 7-chip fixed sequence, and two indices, while the BDS B1C code relies on a 10,243-chip Legendre sequence and two indices. Similarly, by requiring only the storage of the base Legendre sequences (L_p and L_q) alongside three scalar parameters per code, the proposed C.W. family imposes a comparably minimal storage burden. To establish this proposed family, we analyzed the available combinations of prime lengths.

3.3. Searching Optimal Prime Pair

The total of 157 prime pairs satisfy all the aforementioned requirements to form a perfectly balanced family. Since C.W. codes that share the same parent Weil index t_{w1} (and thus the same parent Weil sequence $\boldsymbol{w_p}$) exhibit degraded CCF performance, only a single code per parent index can be included in the final family S. Consequently, we define t_{ACF} as the subset of parent Weil indices that satisfy both the even and odd ACF thresholds, denoted by $\theta_{\mathrm{ACF_E}}$ and $\theta_{\mathrm{ACF_O}}$, respectively. These thresholds correspond specifically to the maximum $\mathrm{ACF_E}$ and $\mathrm{ACF_O}$ of the BDS B1C family, and the cardinality of this subset is denoted by $|t_{\mathrm{ACF}}|$. Similarly, the subset of candidate codes that satisfy $\theta_{\mathrm{ACF_E}}$ and $\theta_{\mathrm{ACF_O}}$ is defined as S_{ACF}, with its cardinality denoted by $|S_{\mathrm{ACF}}|$. Crucially, while $|t_{\mathrm{ACF}}|$ establishes the theoretical maximum size of the final code family, the total number of candidate codes, $|S_{\mathrm{ACF}}|$, plays an equally vital role. Even if two prime pairs exhibit the same $|t_{\mathrm{ACF}}|$, a larger $|S_{\mathrm{ACF}}|$ implies a greater abundance of candidates compliant with ACF per parent index. This increased number of codes increases the probability of passing subsequent CCF validation, leading to a larger final code

 doi:10.20944/preprints202603.1919.v1

family. Therefore, evaluating both $|t_{\mathrm{ACF}}|$ and $|S_{\mathrm{ACF}}|$ for all prime pairs is an essential step to identify the optimal pair that maximizes the final family size.

During the construction of the C.W. family, the parent sequence $\boldsymbol{w_p}$ is shifted due to the insertion of $\boldsymbol{w_q}$, resulting in the separation of the ACF into three regions: the well-aligned region, the shifted region and the inserted region. These three regions change in size depending on the cyclic shift τ ($0 < \tau < N$):

- **Well-aligned region**: This region consists of the parent sequence chips that maintain their original relative cyclic shift of τ. The correlation within this segment behaves as the standard partial-period auto-correlation of the parent sequence $\boldsymbol{w_p}$.
- **Shifted region**: The physical insertion of the q-chip child sequence forces subsequent chips of the parent sequence to be positionally offset. Consequently, during the cyclic wrap-around, a substantial block of the parent sequence is multiplied by an effective relative delay of $\tau + q$ instead of the nominal τ. Like a well-aligned area, the correlation within this segment behaves as the partial-period auto-correlation of the parent Weil sequence $\boldsymbol{w_p}$ with an extra shift.
- **Inserted region**: This region accounts for all correlation interactions involving the inserted child sequence $\boldsymbol{w_q}$. Crucially, when the shift is smaller than the insertion length ($\tau < q$), a segment of the child sequence aligns with its own shifted version, thereby preserving the well-aligned partial auto-correlation properties of $\boldsymbol{w_q}$. The remainder of this region encompasses the cross-correlation between the child sequence $\boldsymbol{w_q}$ and the parent sequence $\boldsymbol{w_p}$, which is bounded within a maximum interaction window of $2q$ chips.

Among the three regions, the correlation performance of the well-aligned and shifted regions has been previously reported [28]. These padded sequences lose the uniform $\mathrm{ACF_E}$ properties of the original Weil sequence and show a degradation of the ACF regardless of the padded sequence (e.g. child sequence). Although no formal error upper bound has been established for this, it is known that significant losses occur for low Weil indices. In contrast, the correlation of the inserted region is dominated by the cross-correlation between the parent and child sequences. As a result, the ACF of the generated C.W. code, denoted as $R_c(\tau)$, can be mathematically formalized as follows:

$$R_c(\tau) = R_{\mathrm{w}}(\tau) + \Delta_{\mathrm{p}}(\tau) + \Delta_{\mathrm{i}}(\tau), \tag{12}$$

where $R_{\mathrm{w}}(\tau)$ denotes the sidelobe of the parent Weil sequence, and $\Delta_{\mathrm{p}}(\tau)$ and $\Delta_{\mathrm{i}}(\tau)$ represent the structural noise caused by padding and the noise caused by the cross-correlation between the child sequence $\boldsymbol{w_q}$ and the parent sequence $\boldsymbol{w_p}$, respectively. The padding noise $\Delta_{\mathrm{p}}(\tau)$ acts as a direct correlation loss. In contrast, insertion noise, $\Delta_{\mathrm{i}}(\tau)$, introduces a dual-faceted impact on correlation properties, which can be analyzed from microscopic and macroscopic perspectives [14]. From a microscopic perspective, the insertion region bounded to the $2q$-chip window provides localized variance. This can be approximated as a random walk model $\mathcal{N}(0, 2q)$, due to the pseudo-random property in Weil sequences. Under a confidence level of 99.7% (3σ), this variance is confined within $\pm 3\sqrt{2q}$. This variance acts as a source of structural diversity, creating statistical opportunities to discover specific code configurations where the noise destructively interferes with and successfully suppresses the degraded correlation sidelobes by insertion. Based on the uniform ideal pseudo-randomness of the Weil family, the probability of suppressing degraded sidelobes is independent of the specific child Weil index t_{w2}. Consequently, the sizes of the valid parent index set ($|t_{\mathrm{ACF}}|$) and the overall candidate code pool ($|S_{\mathrm{ACF}}|$) are proportionally amplified by the number of child Weil indices. In contrast, from a macroscopic perspective, if the insertion length q is extensively increased, the structural disruption pervades the sequence. In this macroscopic limit, the entire code family loses its algebraic Weil properties, which are strictly bounded by $5 + 2\sqrt{N}$, and begins to behave simply as generic random noise. Because the maximum sidelobe of a pure random sequence theoretically scales up to $\approx \sqrt{N \log N}$, this macro-level randomization degrades the overall correlation performance and sharply reduces the number of valid sequence candidates.

 doi:10.20944/preprints202603.1919.v1

To validate these hypotheses, evaluating the entire search space of 157 prime pairs would be ideal but computationally prohibitive. Specifically, the evaluation of a single prime pair required approximately one week of continuous computation, driven by an estimated complexity of $\mathcal{O}(p^2 \cdot q \cdot N \log N)$, where $N = p + q$ is the code length and the $N \log N$ factor reflects the cost of a single FFT-based correlation computation. Therefore, we performed an exhaustive search limited to two prime pairs to investigate the underlying trends in these properties: $(p = 10211, q = 19)$ and $(p = 10159, q = 71)$. (Figure 3).

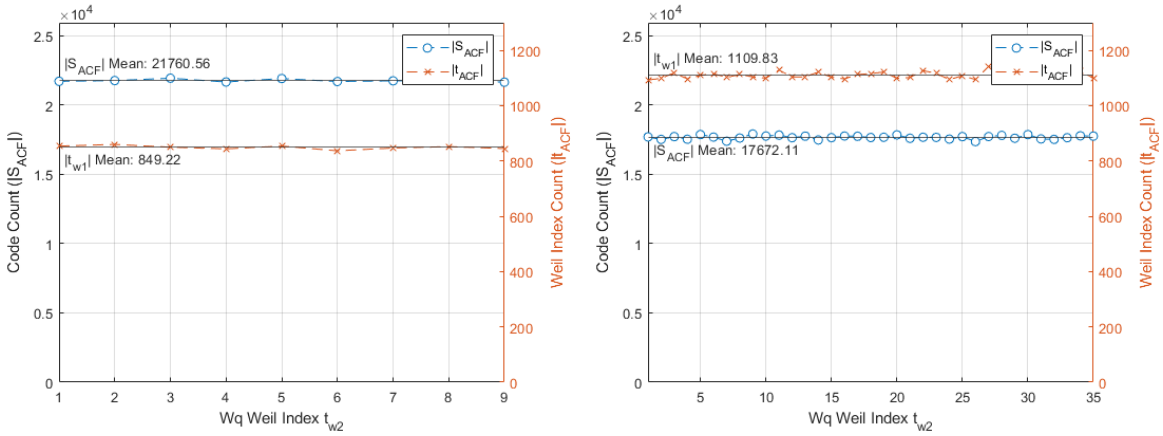

(**a**) (**b**)

Figure 3. Exhaustive search results validating the uniform distributions of $|t_{\mathrm{ACF}}|$ and $|S_{\mathrm{ACF}}|$ across the child Weil index t_{w2} under the BDS B1C ACF threshold for two prime pairs: (**a**) $(p = 10211, q = 19)$; (**b**) $(p = 10159, q = 71)$.

As a result, the results align with our anticipation: for each child Weil index, the prime pair with a higher insertion ratio ($q = 71$) exhibits a smaller candidate size, although it possesses a larger number of valid parent indices for each child Weil index. Furthermore, both the number of ACF-candidate parent Weil indices ($|t_{\mathrm{ACF}}|$) and the size of the ACF-candidate codes ($|S_{\mathrm{ACF}}|$) remain approximately constant in the child Weil index t_{w2}. Based on this validation, we simplified the search space by restricting the child Weil index to a fixed value, namely $t_{\mathrm{w2}} = 1$, across the 28 prime pairs chosen based on their insertion ratios. In this restricted scenario, the number of candidate codes that meet the ACF threshold of the BDS B1C family is denoted $|S_{\mathrm{ACF}}|_1$, and the corresponding number of candidate parent Weil indices is denoted as $|t_{\mathrm{ACF}}|_1$. Given the approximately uniform distribution observed across the child Weil index, the estimated total number of candidate codes, denoted $|\hat{S}_{\mathrm{ACF}}|$, can be expressed as the product of the child Weil index range and $|S_{\mathrm{ACF}}|_1$, as follows:

$$|\hat{S}_{\mathrm{ACF}}| = \left(\frac{q-1}{2}\right)|S_{\mathrm{ACF}}|_1, \tag{13}$$

Generalizing from a single observation induces an estimation error. As demonstrated, we assume an approximately uniform distribution in the child Weil index t_{w2}. Consequently, the potential error can be modeled by defining maximum relative error margins, ϵ_{code} and ϵ_{weil}, for fluctuations of $|S_{\mathrm{ACF}}|_k$ and $|t_{\mathrm{ACF}}|_k$ with respect to their measured values $|S_{\mathrm{ACF}}|_1$ and $|t_{\mathrm{ACF}}|_1$, respectively, as follows:

$$|S_{\mathrm{ACF}}|_k \sim \mathrm{U}(|S_{\mathrm{ACF}}|_1(1-\epsilon_{\mathrm{code}}), |S_{\mathrm{ACF}}|_1(1+\epsilon_{\mathrm{code}})), \tag{14}$$

$$|t_{\mathrm{ACF}}|_k \sim \mathrm{U}(|t_{\mathrm{ACF}}|_1(1-\epsilon_{\mathrm{weil}}), |t_{\mathrm{ACF}}|_1(1+\epsilon_{\mathrm{weil}})), \tag{15}$$

To determine the error margins ϵ_{code} and ϵ_{weil}, we evaluate the coefficients of variation (CV) derived from the distributions for $q = 19$ and $q = 71$. The CV quantifies the relative variability by expressing the standard deviation as a proportion of the mean: specifically, σ_{code} and μ_{code} for the

 doi:10.20944/preprints202603.1919.v1

candidate sizes and σ_{weil} and μ_{weil} for the number of parent Weil indices. These relationships are defined as follows:

$$CV_{\text{code}} = \frac{\sigma_{\text{code}}}{\mu_{\text{code}}}, \qquad CV_{\text{weil}} = \frac{\sigma_{\text{weil}}}{\mu_{\text{weil}}}, \tag{16}$$

Based on our analysis, the calculated CVs for the $(p = 10211, q = 19)$ subset were $CV_{\text{code}} \approx 0.47\%$ and $CV_{\text{weil}} \approx 0.80\%$. For the $(p = 10159, q = 71)$ subset, these values were observed to be $CV_{\text{code}} \approx 0.74\%$ and $CV_{\text{weil}} \approx 1.14\%$. Recognizing this, we established the final error thresholds as $\epsilon_{\text{code}} = 1\%$ and $\epsilon_{\text{weil}} = 1.5\%$.

The analysis reveals that the prime pair $(p = 10091, q = 139)$ produces the largest estimated candidate pool, achieving an estimated total of $|\hat{S}_{\text{ACF}}| = 1,063,980$ and $|t_{\text{ACF}}|_1 = 1,247$ (Figure 4, Table A1). Beyond this peak, both $|\hat{S}_{\text{ACF}}|$ and $|t_{\text{ACF}}|_1$ exhibit a decline. Specifically, for the prime pairs from $(p = 10223, q = 7)$ to $(p = 10091, q = 139)$, the capacity $|\hat{S}_{\text{ACF}}|$ increases with the expanding range of the child Weil index. However, for subsequent pairs from $(p = 10079, q = 151)$ to $(p = 5171, q = 5099)$, $|\hat{S}_{\text{ACF}}|$ begins to decrease because the reduction in $|S_{\text{ACF}}|_1$ outweighs the expanding range of child index.

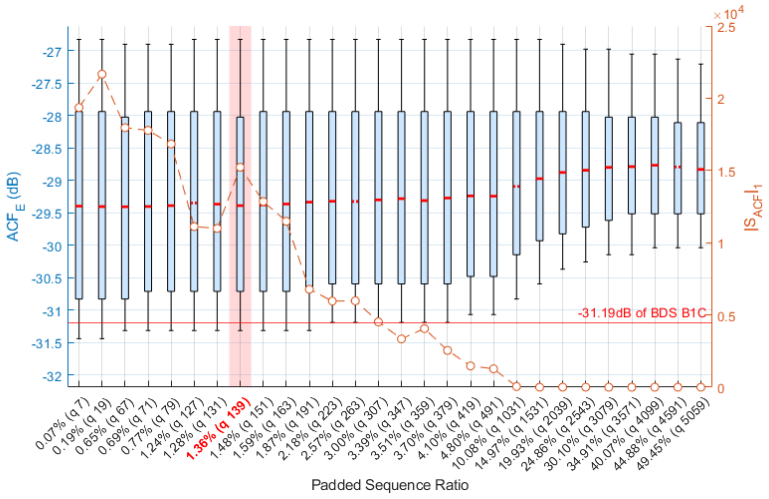

(**a**)

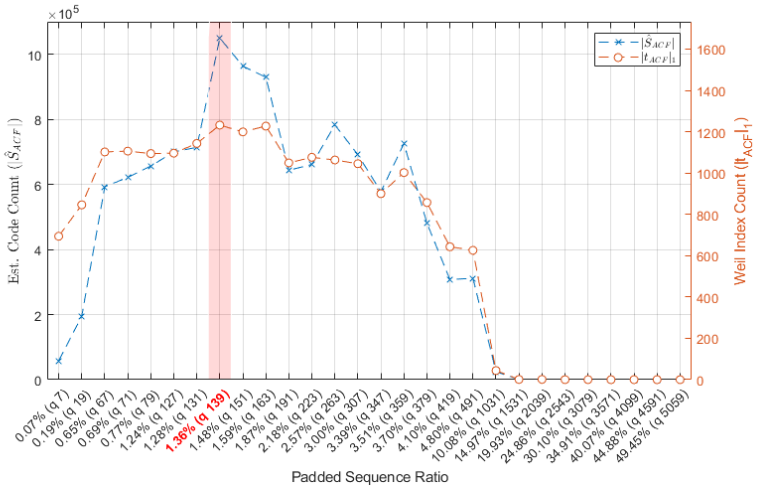

(**b**)

Figure 4. Search results under the restricted environment ($t_{w2} = 1$) demonstrating the maximum candidate pool at $(p = 10091, q = 139)$: (**a**) Boxplot of ACF_E (box: 1σ, whiskers: 2σ) and distribution of $|S_{\text{ACF}}|_1$; (**b**) Distributions of $|\hat{S}_{\text{ACF}}|$ and $|t_{\text{ACF}}|$ across prime pairs.

 doi:10.20944/preprints202603.1919.v1

Specifically, $|\hat{S}_{\mathrm{ACF}}|$ drops to zero after the prime pair $(p = 7687, q = 2543)$. This can be explained by two factors: the expansion of the insertion region and the constraint of the search space. First, as the length of the child sequence (q) increases, the insertion region expands. This macroscopic expansion drives the overall code to perform lower ACF performance of random sequence ($\approx \sqrt{N \log N}$) compared to that of Weil sequence ($5 + 2\sqrt{N}$). Second, this vanishing probability is further compounded by the omitted search space of the exploration process. To achieve computational efficiency, our search architecture reduces the search space from $\mathcal{O}(p^2 \cdot q \cdot N \log N)$ to $\mathcal{O}(p^2 \cdot N \log N)$. Crucially, as q grows, the omitted search dimension becomes larger. As a result, the restricted search space cannot compensate for the plunging survival probability caused by the expanding noise, driving the expected yield of valid candidate codes to absolute extinction.

Based on these findings, we identify that the prime pair $(p = 10091, q = 139)$ contains the largest candidate pool under the ACF constraint. To prove this, we performed an exhaustive search to identify the complete set of ACF-candidate codes for this specific prime pair.The search for ACF-candidate codes for the pair $(p = 10091, q = 139)$ reveals an approximately uniform distribution across the child Weil indices (Figure 5). The ACF search produced a total of 1,059,699 candidate codes ($|S_{\mathrm{ACF}}|$), which is close to the estimated value (1,063,980). On average, each child Weil index encompasses 15,358 candidate codes and 1,245 valid parent Weil indices. In addition, the calculated coefficients of variation are confirmed to be $CV_{\mathrm{code}} \approx 0.72\%$ and $CV_{\mathrm{weil}} \approx 1.08\%$. These empirical results successfully satisfy our predefined conservative error thresholds of $\epsilon_{\mathrm{code}} = 1\%$ and $\epsilon_{\mathrm{weil}} = 1.5\%$, validating our estimation methodology and the restricted search strategy.

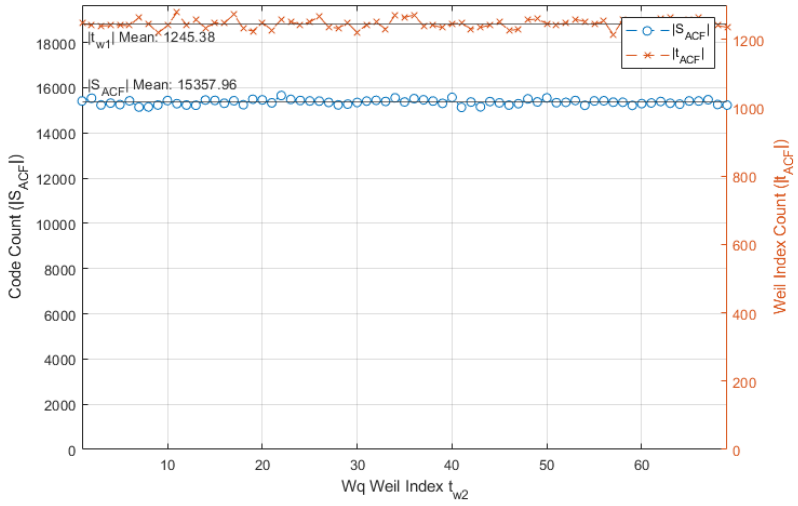

Figure 5. Distributions of valid parent Weil indices ($|t_{\mathrm{ACF}}|$) and candidate codes ($|S_{\mathrm{ACF}}|$) for the pair $(p = 10091, q = 139)$ as a function of the child Weil index t_{w2}

3.4. Optimal Code Search Procedure

In this section, we present the two-step procedure used to construct the final valid code set S. Recognizing that smaller Weil indices often lead to degraded odd autocorrelation performance ($\mathrm{ACF_O}$) [28], the overall search is intentionally executed in descending order of the parent Weil index, starting from $t_{\mathrm{w1}} = 5045$.

The first step consists of an ACF search procedure designed to identify a preliminary subset, S_{ACF}, comprising all configurable C.W. codes that satisfy the predefined ACF thresholds, $\theta_{\mathrm{ACF_E}}$ and $\theta_{\mathrm{ACF_O}}$ (Algorithm 1). The function genPRN$(t_{\mathrm{w1}}, t_{\mathrm{w2}}, i_{\mathrm{p}})$ generates a candidate code sequence based on the parent Weil index t_{w1}, the child Weil index t_{w2}, and the insertion index i_{p}. Subsequently, the function acf_sl$(\boldsymbol{c})$ calculates the $\mathrm{ACF_E}$ and $\mathrm{ACF_O}$ of the proposed candidate code $\boldsymbol{c}$. If both values do not exceed their respective thresholds, the code $\boldsymbol{c}$ is appended to the set S_{ACF}.

The second step is a CCF search procedure that filters S_{ACF} to form the final optimal code set S (Algorithm 2). First, codes within S_{ACF} that share the same parent Weil index t_{w1} are sorted in

 doi:10.20944/preprints202603.1919.v1

ascending order of their maximum ACF sidelobe ($\mathrm{ACF_M}$). Following this, the function $\mathrm{ccf\_sl}(\boldsymbol{c}, \boldsymbol{s})$ computes the $\mathrm{CCF_E}$ and $\mathrm{CCF_O}$ between a new candidate code $\boldsymbol{c}$ drawn from the sorted S_{ACF} and all reference codes $\boldsymbol{s}$ currently residing in S. If both CCF values for all such pairs are less than or equal to the thresholds $\theta_{\mathrm{CCF_E}}$ and $\theta_{\mathrm{CCF_O}}$, the candidate $\boldsymbol{c}$ is verified as an optimal code and is appended to the final set S.

Algorithm 1: The ACF-Candidate Code Search Procedure

Input : (i) Fixed Parameter p, q, ϕ
(ii) ACF Threshold $\theta_{\mathrm{ACF_E}}, \theta_{\mathrm{ACF_O}}$
Output: (i) ACF-candidate Set S_{ACF}

$S_{\mathrm{ACF}} \leftarrow \emptyset$;
`// Stage 01: Auto Correlation Search`
for $\frac{(p-1)}{2} \geq w_1 \geq 1$ **do**
  for $1 \leq w_2 \leq \frac{(q-1)}{2}$ **do**
    for $1 \leq i_{\mathrm{p}} \leq p$ **do**
      $\boldsymbol{c} = \mathrm{genPRN}(w_1, w_2, i_{\mathrm{p}})$;
      $[\mathrm{acf_e}, \mathrm{acf_o}] = \mathrm{acf\_sl}(\boldsymbol{c})$;
      if $\mathrm{acf_e} \leq \theta_{\mathrm{ACF_E}} \wedge \mathrm{acf_o} \leq \theta_{\mathrm{ACF_O}}$ **then**
        $S_{\mathrm{ACF}} \leftarrow S_{\mathrm{ACF}} \cup \{(w_1, w_2, i_{\mathrm{p}})\}$;
      end
    end
  end
end
return S_{ACF};

Algorithm 2: The Final Optimal Code Search Procedure

Input : (i) Fixed Parameter p, q, ϕ
(ii) CCF Threshold $\theta_{\mathrm{CCF_E}}, \theta_{\mathrm{CCF_O}}$
(iii) ACF-candidate Set S_{ACF}
Output: (i) Code Set S

$S \leftarrow \emptyset$;
$\boldsymbol{s} \leftarrow \emptyset$;
`// Stage 02: Cross Correlation Search`
for $\frac{(p-1)}{2} \geq t_{\mathrm{w1}} \geq 1$ **do**
  `// Extract and sort candidates for current` t_{w1}
  $S_{\mathrm{w1}} \leftarrow \{(w_1, w_2, i_{\mathrm{p}}) \in S_{\mathrm{ACF}} \mid w_1 = t_{\mathrm{w1}}\}$;
  Sort S_{w1} in ascending order based on their $\mathrm{ACF_M}$ values;
  `// Iterate through sorted candidates directly`
  foreach $(w_1, w_2, i_{\mathrm{p}}) \in S_{\mathrm{w1}}$ **do**
    $\mathrm{ccf_e} \leftarrow \emptyset$;
    $\mathrm{ccf_o} \leftarrow \emptyset$;
    $\boldsymbol{c} = \mathrm{genPRN}(w_1, w_2, i_{\mathrm{p}})$;
    for $1 \leq i_{\mathrm{c}} \leq |S|$ **do**
      $[\mathrm{ccf_e}^{(i_{\mathrm{c}})}, \mathrm{ccf_o}^{(i_{\mathrm{c}})}] = \mathrm{ccf\_sl}(\boldsymbol{c}, \boldsymbol{s}^{(i_{\mathrm{c}})})$;
    end
    if $\max(\mathrm{ccf_e}) \leq \theta_{\mathrm{CCF_E}} \wedge \max(\mathrm{ccf_o}) \leq \theta_{\mathrm{CCF_O}}$ **then**
      $S \leftarrow S \cup \{(w_1, w_2, i_{\mathrm{p}})\}$;
      $\boldsymbol{s} \leftarrow \boldsymbol{s} \cup \{\boldsymbol{c}\}$;
    end
  end
end
return S;

 doi:10.20944/preprints202603.1919.v1

4. Result

The search procedure adopts the maximum correlation performance of the BDS B1C family as its baseline, relaxing the CCF threshold until the target family size is achieved. This experimental design is motivated by the fact that the degradation caused by the worst-case CCF of sequences can be mitigated by allocating these pairs to geographically isolated satellites or multiplexing them onto orthogonal phases. Based on this approach, two distinct threshold criteria were established:

- Threshold A (Thr.A): Applies the ACF threshold (-31.19 dB for both $\theta_{\mathrm{ACF_E}}$ and $\theta_{\mathrm{ACF_O}}$) and the CCF thresholds (-27.29 dB for both $\theta_{\mathrm{CCF_E}}$ and $\theta_{\mathrm{CCF_O}}$) of the BDS B1C family.
- Threshold B (Thr.B): Maintains the ACF threshold (-31.19 dB for both $\theta_{\mathrm{ACF_E}}$ and $\theta_{\mathrm{ACF_O}}$) of the BDS B1C family but relaxes the CCF threshold (-27.21 dB for $\theta_{\mathrm{CCF_E}}$, -26.22 dB for $\theta_{\mathrm{CCF_O}}$) to match that of the GPS L1C family.

Consequently, Thr.A yielded a family of 254 C.W. codes, roughly twice the number of codes compared to the existing BDS B1C family (126 codes) under the exact same correlation thresholds. The Thr.B allowed us to construct the family of 608 codes even if enforces a better ACF threshold than the GPS L1C family. For the purpose of subsequent analysis, these proposed families are denoted as C.W. (Thr.A) and C.W. (Thr.B), respectively.

The Cumulative Distribution Functions (CDFs) of the correlation performance for the proposed C.W. families are closely aligned with those of the BDS B1C family (Figure 6). As before, only the BPSK modulation and the Doppler effect of 0 Hz were considered. As intended, the proposed C.W. family is robust in odd correlation scenarios, thus achieving better correlation performance compared to that of the NavIC L1 SPS. Nevertheless, the structural limitations of the insertion and truncation processes lead to a degradation in the performance of CCF compared to the NavIC L1 SPS. A difference is observed when comparing the odd CCF of the C.W. (Thr.B) family to that of the GPS L1C family. The C.W. (Thr.B) family exhibits a better CCF distribution than the GPS L1C family. Although the C.W. (Thr.B) family inserts 139-chip codes, which is 132 chips longer than the 7-chip insertion used in GPS L1C family, it selectively utilizes 69 distinct child Weil sequences. Consequently, an average of 8.81 codes (with a median of 9) share the same child Weil code within the C.W. (Thr.B) family. This selective insertion mitigates inter-family interference, directly resulting in the observed enhancement of the overall CCF performance.

Table 6 summarizes the performance of the code families. The results demonstrate that the proposed C.W. code families benefit from their massively expanded family sizes (254 for Thr. A and 608 for Thr. B). Specifically, when evaluating the best 126 codes (Top 126) to match the baseline performance of the BDS B1C family, the proposed C.W. (Thr. A) achieves a superior $\mathrm{ACF_M}$ of -31.44 dB, outperforming all conventional RNSS signals. In the 95% and 99% top evaluations, both the C.W. families exhibit $\mathrm{ACF_M}$ values of -31.22 dB and -31.19 dB, respectively, approximately matching the baseline of the BDS B1C family. The $\mathrm{ACF_M}$ of the NavIC L1 SPS is evaluated at -30.66 dB. As intended, the C.W. family explicitly mitigates the ACF degradation conventionally caused by odd correlation scenarios.

Although previous performance comparisons across different code families assumed a 0 Hz Doppler frequency, the proposed code family is designed for LEO-PNT constellations. Consequently, the correlation performance degradation induced by the high Doppler frequency must be analyzed. For the ACF, the impact of Doppler frequency is relatively minor, as the performance is dictated by the residual Doppler within the maximum likelihood estimation. However, the Cross Ambiguity Function (CAF) requires thorough investigation under Doppler-strained conditions and all code delays and phase inversion combinations. Nevertheless, conducting an exhaustive CAF analysis across the entire Pulsar Doppler range (± 33 kHz) for all possible code delays ($0 \leq \tau < N$), phase inversions, and code combinations is computationally impossible.

Based on this practical limitation, we constructed a representative subset of 100 code combinations from the C.W. (Thr.B) family. To ensure a worst-case evaluation, this subset comprises 30 pairs randomly selected from the 287 combinations that exhibit the maximum $\mathrm{CCF_E}$, 30 pairs from the 37 combinations with the maximum $\mathrm{CCF_O}$, and 40 pairs randomly chosen from the remainder. Assuming

 doi:10.20944/preprints202603.1919.v1

BPSK modulation and an oversampling factor of 8 samples per chip, the correlation performance was evaluated across a Doppler frequency range of ± 40 kHz with a resolution step of 10 kHz without considering the Doppler rate. Furthermore, to manage the computational complexity, the evaluation of the odd CCF scenario was limited to the specific time delay that yields the maximum CCF_O.

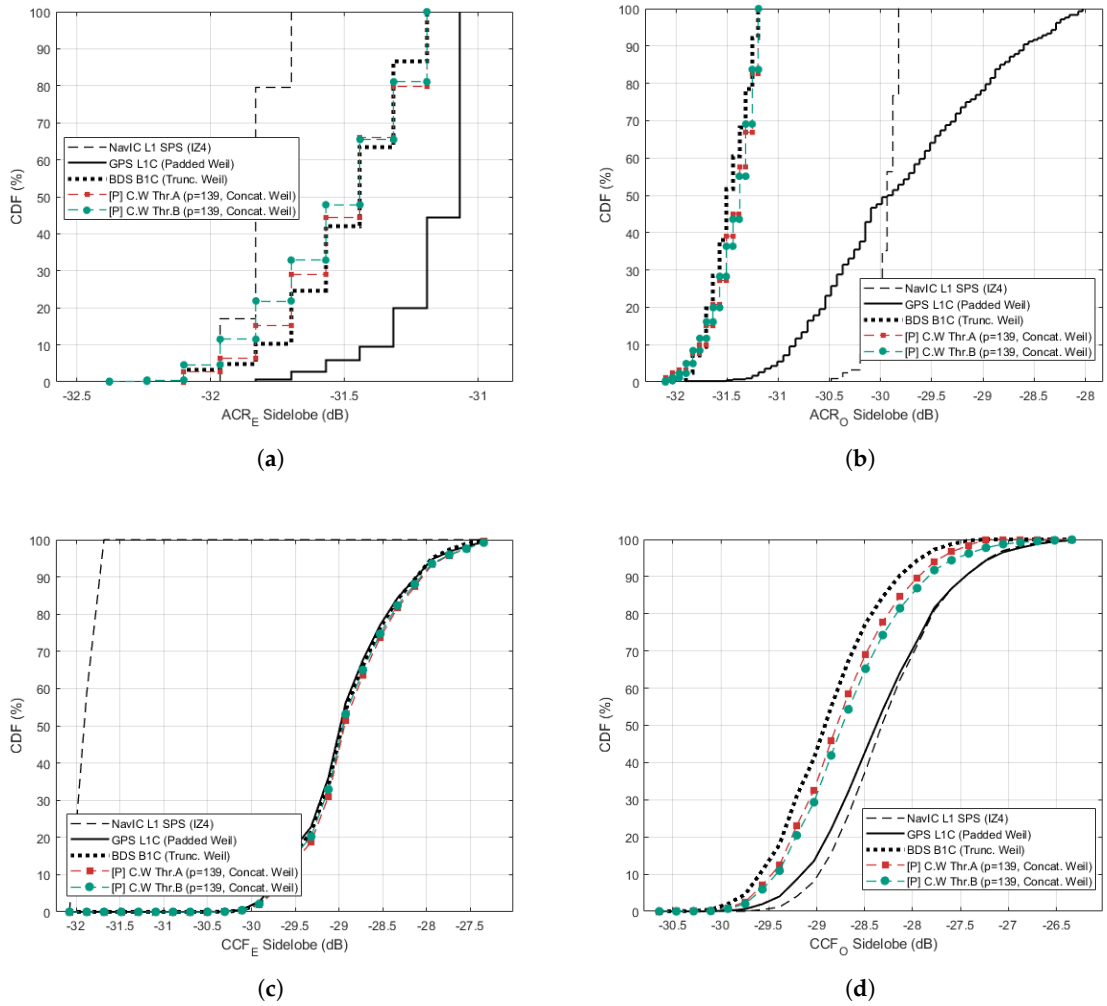

Figure 6. Cumulative Distribution Functions (CDFs) of correlation performance comparing the proposed C.W. families with GPS L1C, BDS B1C, and NavIC L1 SPS families: (**a**) CDF of ACF_E; (**b**) CDF of ACF_O; (**c**) CDF of CCF_E; (**d**) CDF of CCF_O;

Table 6. Comparison of correlation sidelobes demonstrating the enhanced CCF performance of the proposed C.W. families against GPS L1C, BDS B1C and NavIC SPS.

Signal Type	Family Size	ACF_M (dB)				CCF_M (dB)		
		Top. 126	Top. 50%	Top. 95%	Top. 99%	Top. 50%	Top. 95%	Top. 99%
GPS L1C	420	−30.74	−30.49	−29.53	−29.41	−28.62	−27.81	−27.47
BDS B1C	126	−31.19	−31.50	−31.22	−31.19	−28.90	−28.19	−27.94
NavIC L1 SPS	128	−30.66	−30.78	−30.66	−30.66	−29.77	−28.95	−28.59
[P] C.W. Thr.A	254	−31.44	−31.44	−31.22	−31.19	−28.80	−28.07	−27.79
[P] C.W. Thr.B	608	−31.63	−31.47	−31.22	−31.19	−28.78	−27.98	−27.63

* Note 1: [P] denotes the proposed method in this work.

The experimental procedure is structured to capture the cell from the worst-case CAF profile. Each individual CAF is computed over an integration interval of a code period with a Doppler frequency

 doi:10.20944/preprints202603.1919.v1

bin resolution of 50 Hz. Once the CAF is derived for a designated code pair at a specific Doppler frequency, it is compared element-wise against a globally accumulated CAF matrix, retaining only the maximum value in each delay-Doppler cell. Because we evaluated 100 code combinations across 9 discrete Doppler frequencies, this procedure aggregated a total of 900 even CAFs and 900 odd CAFs. Consequently, each cell in the final composite even and odd CAF matrices stores the absolute maximum correlation value observed across all iterations.

The analysis reveals that within the CAF profile, more than 99.99% of the evaluated search space satisfies the correlation thresholds (Figure 7). For the even correlation scenario, 10 cells distributed across 10 frequency bins fail to satisfy the search threshold of -27.21 dB. The peak $\mathrm{CCF_E}$ of these non-ideal cells is -26.64 dB, exceeding the threshold by approximately 0.47 dB. To ensure system integrity, these specific pairs should either be excluded from the primary code set or, if utilized, physically or logically isolated. In contrast, the odd CAF profile demonstrates that all evaluated cells successfully satisfy their respective threshold of -26.22 dB.

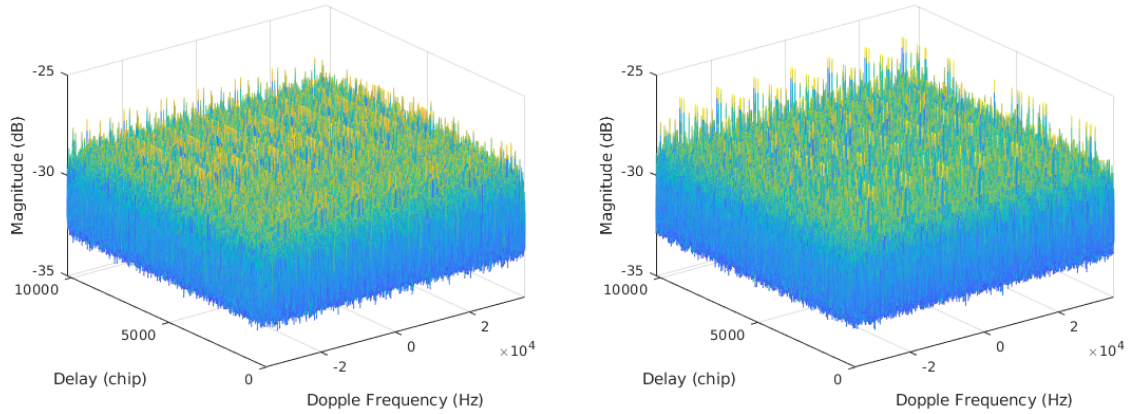

Figure 7. Aggregated worst-case cross-ambiguity function (CAF) profiles evaluated over 100 code combinations and 9 Doppler frequencies: (**a**) Composite Even CAF; (**b**) Composite Odd CAF.

The complete set of generation parameters, the parent Weil index t_{w1}, the child Weil index t_{w2}, and the insertion index i_p, for all sequences in both the C.W. (Thr.A) and C.W. (Thr.B) families is publicly available at GitHub for further verification and research.

5. Discussion

Although the proposed Concatenated Weil (C.W.) code family significantly expands the family size of sequence while maintaining comparable correlation performance to existing RNSS signals, several limitations in the current design and evaluation methodology must be addressed in future work.

In this paper, the structural noise components introduced by the insertion are approximated as $\Delta_p(\tau)$ and $\Delta_i(\tau)$, respectively. Although this assumption is supported by previous studies and the inherent pseudo-random properties of Weil sequences, it remains a theoretical approximation. The concatenation of two deterministic sequences does not guarantee perfect randomness. Depending on specific combinations of prime pairs and insertion indices (i_p), unintended constructive interference (singularities) could occur, leading to a degradation in correlation performance. Future studies should mathematically formulate the exact upper and lower bounds of $\Delta_p(\tau)$ and $\Delta_i(\tau)$ to quantify these worst-case scenarios and provide a deterministic guarantee against such structural singularities.

Furthermore, the CAF evaluation was conducted under the assumption of BPSK modulation. However, because the actual Pulsar X5 signal employs EFQPSK, a further correlation analysis that incorporates this specific modulation scheme is required for real-world deployment. This analysis, grounded in the actual signal specifications, is essential to evaluate the suitability of the proposed

 doi:10.20944/preprints202603.1919.v1

code family. Ultimately, this subsequent verification will confirm its practical viability in operational LEO-PNT environments.

6. Conclusion

In this study, we addressed the critical capacity limitations of PN families in emerging LEO-PNT constellations. Although traditional RNSS operates with a limited number of satellites, dense LEO-PNT constellations require hundreds of unique codes. To overcome these challenges, we proposed the C.W. code family, designed to expand family size while maintaining correlation performance. The proposed C.W. family is constructed via prime concatenation motivated by the Goldbach conjecture, which states that every even integer greater than 2 can be expressed as the sum of two primes.

Among the 157 prime pairs capable of generating balanced codes, we select the optimal prime pair ($p = 10091, q = 139$) based on the estimated ACF-candidate metrics. As a result, we obtained 254 sequences using Threshold A, which adopts the maximum correlation performance of the BDS B1C family, and 608 sequences using Threshold B, based on the maximum ACF performance of the BDS B1C family and the maximum CCF performance of GPS L1C family.

Notably, while the C.W. (Thr. A) family shares the same correlation thresholds as the BDS B1C family, it provides an additional 128 sequences compared to the BDS B1C family (126) while maintaining comparable correlation performance. Furthermore, although the GPS L1C family adopted a more relaxed ACF threshold, the C.W. (Thr. B) family contains an additional 188 sequences compared to the GPS L1C family (420). The C.W. (Thr. B) family also exhibits better CCF performance over the GPS L1C family, with an overall improvement of 0.25 dB, and a more significant gain of 0.50 dB in odd-correlation scenarios. This enhanced performance and capacity are primarily attributed to the selective insertion architecture of the C.W. family, selecting one insertion code among the 69 child sequences.

Although this study focused on the single prime pair estimated to yield the largest size, the proposed methodology is applicable to the valid prime pairs capable of generating balanced codes. Furthermore, because this concatenation approach enables the highly flexible construction of code families with any even length, it transcends the period evaluated in this paper. Ultimately, we anticipate that this novel generation architecture will have a profound impact on the design paradigm of future LEO-PNT spreading code families.

Author Contributions: Conceptualization, J.Y. and S.Y.; methodology, S.Y.; software, J.Y.; validation, J.Y., S.Y., G.J. and S.K.; formal analysis, J.Y.; investigation, J.Y.; resources, J.Y.; data curation, J.Y. and S.Y.; writing—original draft preparation, J.Y.; writing—review and editing, S.Y., G.J. and S.K.; visualization, J.Y.; supervision, S.Y., G.J. and S.K.; project administration, S.K.; funding acquisition, J.M. and G.J. All authors have read and agreed to the published version of the manuscript.

Funding: This research was supported by funding from Korea government (KASA, Korea AeroSpace Administration) (grant number RS-2022-00165802).

Institutional Review Board Statement: Not applicable

Informed Consent Statement: Not applicable

Data Availability Statement: The MATLAB simulation codes for the proposed Concatenated Weil (C.W.) family design is openly available in [GitHub] at https://github.com/abcbank/Concatenated-Weil-PN-Code.

Conflicts of Interest: The funders had no role in the design of the study; in the collection, analyses, or interpretation of data; in the writing of the manuscript; or in the decision to publish the results.

 doi:10.20944/preprints202603.1919.v1

Appendix A

Table A1. Summary of the prime pairs (p, q) used in the experiment and the resulting candidate metrics ($|\hat{S}_{\mathrm{ACF}}|$ and $|t_{\mathrm{ACF}}|_1$).

Index	p	q	Insert Ratio (%)	$\lvert\hat{S}_{\mathrm{ACF}}\rvert$	$\lvert t_{\mathrm{ACF}}\rvert_1$
01	10,223	7	0.07	58,056	694
02	10,211	19	0.19	194,949	846
03	10,163	67	0.65	592,647	1,102
04	10,159	71	0.69	622,160	1,106
05	10,151	79	0.77	656,487	1,094
06	10,103	127	1.24	700,308	1,096
07	10,099	131	1.28	708,955	1,143
08	10,091	139	1.36	1,063,980	1,247
09	10,079	151	1.48	963,750	1,199
10	10,067	163	1.59	929,799	1,227
11	10,039	191	1.87	643,815	1,049
12	10,007	223	2.18	661,560	1,076
13	9,967	263	2.57	783,118	1,063
14	9,923	307	3.00	691,560	1,045
15	9,883	347	3.39	577,993	900
16	9,871	359	3.51	725,845	1,002
17	9,851	379	3.70	481,194	857
18	9,811	419	4.10	307,648	643
19	9,739	491	4.80 (≈ 5)	311,640	626
20	9,199	1,031	10.08 (≈ 10)	24,205	44
21	8,699	1,531	14.97 (≈ 15)	765	1
22	8,191	2,039	19.93 (≈ 20)	1,019	1
23	7,687	2,543	24.86 (≈ 25)	0	0
24	7,151	3,079	30.10 (≈ 30)	0	0
25	6,659	3,571	34.91 (≈ 35)	0	0
26	6,131	4,099	40.07 (≈ 40)	0	0
27	5,639	4,591	44.88 (≈ 45)	0	0
28	5,171	5,099	49.45 (≈ 50)	0	0

References

1. Morton, Y.J.; van Diggelen, F.; Spilker, J.J., Jr.; Parkinson, B.W., Eds. *Position, Navigation, and Timing Technologies in the 21st Century: Integrated Satellite Navigation, Sensor Systems, and Civil Applications*; Wiley-IEEE Press: Hoboken, NJ, USA, 2021. [CrossRef]
2. Ge, H.; Li, B.; Jia, S.; Nie, L.; Wu, T.; Yang, Z.; Shang, J.; Zheng, Y.; Ge, M. LEO Enhanced Global Navigation Satellite System (LeGNSS): Progress, Opportunities, and Challenges. *Geo-spatial Inf. Sci.* **2022**, *25*, 1–13. [CrossRef]
3. FrontierSI. *State of the Market Report, Low Earth Orbit Positioning Navigation and Timing – 2024 Edition*; FrontierSI: Melbourne, Australia, 2024. Available online: [Online] (accessed on 26 February 2026).

 doi:10.20944/preprints202603.1919.v1

4. Su, J.; Su, J.; Yi, Q.; Wu, C.; Hou, W. Design and performance evaluation of a novel ranging signal based on an LEO satellite communication constellation. *Geo-Spat. Inf. Sci.* **2023**, *26*, 107–124. [CrossRef]
5. Reid, T.G.R.; Gala, M.; Favreau, M.; Kriezis, A.; O'Meara, M.; Pant, A.; Tarantino, P.; Youn, C. Xona Pulsar Compatibility with GNSS. In Proceedings of the 38th International Technical Meeting of the Satellite Division of The Institute of Navigation (ION GNSS+ 2025), Baltimore, MD, USA, 8–12 September 2025. [CrossRef]
6. Leclère, J.; Marathe, T.; Reid, T.G.R. Insights into Xona Pulsar LEO PNT: Constellation, Signals, and Receiver Design. In Proceedings of the 38th International Technical Meeting of the Satellite Division of The Institute of Navigation (ION GNSS+ 2025), Baltimore, MD, USA, 8–12 September 2025; pp. 3008–3096. [CrossRef]
7. Ahmed, F.; Shannon, P.; Schmitt, G.; Goparaju, A. TrustPoint LEO PNT: Evaluating Geometric Strength, Urban Availability, and Multi-Constellation Integration. In Proceedings of the 38th International Technical Meeting of the Satellite Division of The Institute of Navigation (ION GNSS+ 2025), Baltimore, MD, USA, 8–12 September 2025; pp. 2332–2345. [CrossRef]
8. Yang, L. In-orbit Testing Results of CENTISPACE LEO Augmentation Experimental Satellites. In Proceedings of the 17th Meeting of the International Committee on Global Navigation Satellite Systems (ICG-17), Madrid, Spain, 15–20 October 2023. Available online: [Online] (accessed on 26 February 2026).
9. Prieto Cerdeira, R.; Giordano, P.; Cordero, M.; Grec, F.; Le Priellec, A.; Sarnadas, R.; Breeuwer, E.; Ait-Mohammed, N.; Anghileri, M. Enhancing GNSS with a Low Earth Orbit layer: Celeste In-Orbit Demonstration Mission. In Proceedings of the 38th International Technical Meeting of the Satellite Division of The Institute of Navigation (ION GNSS+ 2025), Baltimore, MD, USA, 8–12 September 2025; pp. 2322–2331. [CrossRef]
10. Hong, J.; Tu, R.; Zhang, P.; Zhang, R.; Han, J.; Fan, L.; Wang, S.; Lu, X. GNSS rapid precise point positioning enhanced by low Earth orbit satellites. *Satell. Navig.* **2023**, *4*, 11. [CrossRef]
11. Ge, H.; Meng, G.; Li, B. LEO enhanced GNSS (LeGNSS) precise point positioning with emphasis on model comparison. *Adv. Space Res.* **2024**, *74*, 2156–2168. [CrossRef]
12. Xu, S.; Yang, Q.; Du, X.; Xu, X.; Zhao, Q.; Yang, L.; Qin, Y.; Guo, J. Multi-GNSS Precise Point Positioning enhanced by the real navigation signals from CENTISPACE^{TM} LEO mission. *Adv. Space Res.* **2024**, *73*, 4175–4186. [CrossRef]
13. Gala, M.; Reid, T.G.R.; Marathe, T.; Sibois, A.; Tantry, S.; Gunning, K.; Bisnath, S. The rise of LEO PNT. *GPS World* **2026**. Available online: [Online] (accessed on 26 February 2026).
14. Lam, A.W.; Tantaratana, S. *Theory and Applications of Spread-Spectrum Systems: A Self-Study Course*; IEEE: Piscataway, NJ, USA, 1994.
15. Gold, R. Optimal binary sequences for spread spectrum multiplexing. *IEEE Trans. Inf. Theory* **1967**, *13*, 619–621. [CrossRef]
16. Kasami, T. *Weight distribution formula for some class of cyclic codes*, Technical Report R-285; Coordinated Science Laboratory, University of Illinois: Urbana, IL, USA, 1966. [Report]
17. Olsen, J.D.; Scholtz, R.A.; Welch, L.R. Bent-function sequences. *IEEE Trans. Inf. Theory* **1982**, *28*, 858–864. [CrossRef]
18. No, J.S.; Kumar, P.V. A new family of binary pseudorandom sequences having optimal periodic correlation properties and large linear span. *IEEE Trans. Inf. Theory* **1989**, *35*, 371–379. [CrossRef]
19. Hammons, A.R., Jr.; Kumar, P.V.; Calderbank, A.R.; Sloane, N.J.A.; Solé, P. The Z_4-linearity of Kerdock, Preparata, Goethals, and related codes. *IEEE Trans. Inf. Theory* **1994**, *40*, 301–319. [CrossRef]
20. Rushanan, J.J. Weil sequences: A family of binary sequences with good correlation properties. In Proceedings of the 2006 IEEE International Symposium on Information Theory, Seattle, WA, USA, 9–14 July 2006; pp. 1648–1652. [CrossRef]
21. Space Systems Command. *NAVSTAR GPS Space Segment/Navigation User Interfaces (IS-GPS-200, Revision N)*; Space Systems Command: El Segundo, CA, USA, 2022. Available online: [Online] (accessed on 23 February 2026).
22. Space Systems Command. *NAVSTAR GPS Space Segment/User Segment L5 Interfaces (IS-GPS-705, Revision J)*; Space Systems Command: El Segundo, CA, USA, 2022. Available online: [Online] (accessed on 23 February 2026).
23. Space Systems Command. *NAVSTAR GPS Space Segment/User Segment L1C Interfaces (IS-GPS-800, Revision J)*; Space Systems Command: El Segundo, CA, USA, 2022. Available online: [Online] (accessed on 23 February 2026).

 doi:10.20944/preprints202603.1919.v1

24. China Satellite Navigation Office. *BeiDou Navigation Satellite System Signal In Space Interface Control Document Open Service Signal B1C (Version 1.0)*; China Satellite Navigation Office: Beijing, China, 2017. Available online: [Online] (accessed on 23 February 2026).
25. Indian Space Research Organisation (ISRO). *NavIC Signal in Space ICD for Standard Positioning Service in L1 Frequency*, Version 1.0; ISRO: Bengaluru, India, 2023. Available online: [Online] (accessed on 23 February 2026).
26. Fontana, R.D.; Cheung, W.; Novak, P.M.; Stansell, T.A. The New L2 Civil Signal. In Proceedings of the 14th International Technical Meeting of the Satellite Division of The Institute of Navigation (ION GPS 2001), Salt Lake City, UT, USA, 11–14 September 2001; pp. 617–631. [Publisher]
27. Spilker, J.J., Jr.; Van Dierendonck, A.J. Proposed new L5 civil GPS codes. *Navigation* **2001**, *48*, 135–144. [Publisher]
28. Rushanan, J.J. The spreading and overlay codes for the L1C signal. *Navigation* **2007**, *54*, 43–51. [CrossRef]
29. Sun, X. Performance analysis of BDS-3 B1C and GPS L1C data/pilot component pseudo random noise codes. *J. Appl. Geod.* **2018**, *12*, 267–278. [CrossRef]
30. Kumar, P.V.; Dharmappa, D.; Mishra, S. Interleaved Z_4-Linear Sequences With Low Correlation for Global Navigation Satellite Systems. *IEEE Trans. Inf. Theory* **2024**, *70*, 2224–2240. [CrossRef]
31. Wang, W.; Tian, Y.; Bian, L.; Wang, G.; Meng, Y.; Zhang, L. A Novel Satellite PRN Code Assignment Method Based on Improved RLF Algorithm. *Sensors* **2022**, *22*, 5538. [CrossRef]
32. Oliveira e Silva, T.; Herzog, S.; Pardi, S. Empirical verification of the even Goldbach conjecture and computation of prime gaps up to $4 \cdot 10^{18}$. *Math. Comp.* **2014**, *83*, 2033–2060. [CrossRef]
33. Zhang, G.; Zhou, Q. Pseudonoise codes constructed by Legendre sequence. *Electron. Lett.* **2002**, *38*, 376–377. [CrossRef]
34. Gauss, C.F. *Disquisitiones Arithmeticae*; Fleischer: Leipzig, Germany, 1801.
35. Ding, C.; Pei, D.; Salomaa, A. *Chinese Remainder Theorem: Applications in Computing, Coding, Cryptography*; World Scientific: Singapore, 1996. [CrossRef]
36. Taylor, F.B. Simulation Study of Digitized Enhanced Feher Quadrature Phase Shift Keying (EFQPSK). Master's Thesis, University of Tennessee, Knoxville, TN, USA, 2006. [Online]
37. Salos, D.; Garcia-Pena, A.; Julien, O.; Ries, L.; Grelier, T. Investigation of CSK as a Candidate for Future GNSS Signals. In Proceedings of the 6th European Workshop on GNSS Signals and Signal Processing, Munich, Germany, 5–6 December 2013. [Publisher]
38. Space Segment | GPS.gov. Available online: [Online] (accessed on 23 February 2026).
39. van Diggelen, F. *A-GPS: Assisted GPS, GNSS, and SBAS*; Artech House: Boston, MA, USA, 2009.